Unravelling the collagen network of the arterial wall

Beenakker, J.W.M.

4 Defects in collagen organisation in abdominal aneurysms

This chapter has been published as:
Distinct defects in collagen microarchitecture underlie vessel-wall failure in advanced abdominal aneurysms and aneurysms in Marfan syndrome
J. H. N. Lindeman, B. A. Ashcroft, J. W. M. Beenakker, M. van Es, N. B. R. Koekkoek, F. A. Prins, J. F. Tielemans, H. Abdul-Hussien, R. A. Bank and T. H. Oosterkamp
Proceedings of the National Academy of Sciences 107:862, 2010

4.1 Abstract

An aneurysm of the aorta is a common pathology characterized by segmental weakening of the artery. Although it is generally accepted that the vessel-wall weakening is caused by an impaired collagen metabolism, a clear association has been demonstrated only for rare syndromes such as the vascular type Ehlers-Danlos syndrome. Here we show that vessel-wall failure in growing aneurysms of patients who have aortic abdominal aneurysm (AAA) or Marfan syndrome is not related to a collagen defect at the molecular level. On the contrary our findings indicate similar (Marfan) or even higher collagen concentrations (AAA) and increased collagen cross-linking in the aneurysms. Using 3D confocal imaging we show that the two conditions are associated with profound defects in collagen microarchitecture. Reconstructions of normal vessel wall show that adventitial collagen fibers are organized in a loose braiding of collagen ribbons. These ribbons encage the vessel, allowing the vessel to dilate easily but preventing overstretching. AAA and aneurysms in Marfan syndrome show dramatically altered collagen architectures with loss of the collagen knitting. Evaluations of the functional characteristics by atomic force microscopy showed that the wall has lost its ability to stretch easily and revealed a second defect: although vascular collagen in normal aortic wall behaves as a coherent network, in AAA and Marfan tissues it does not. As a result, mechanical forces loaded on individual fibers are not distributed over the tissue. These studies demonstrate that the mechanical properties of tissue are strongly influenced by collagen microarchitecture and that perturbations in the collagen networks may lead to mechanical failure.

4.2 Introduction

Aortic aneurysms are localized dilatations of the aortic wall that are caused by segmental weakening of the vessel wall. Although aneurysms generally are without clinical symptoms, larger aneurysms may rupture, and bleeding from a ruptured aneurysm is responsible for more than 15,000 annual deaths in the United States alone.[1]

Aneurysm formation relates to a primary or secondary (acquired) defect in the matrix structures supporting the vessel wall resulting in attenuation and ultimate failure of the vessel wall.[2] Although extensive loss of medial elastin traditionally is considered the hallmark of aneurysm formation, it now is acknowledged that aneurysmal growth and ultimate rupture relate to impaired collagen homeostasis.[2] Remarkably, although numerous studies have looked for putative quantitative changes in aortic collagen, results reported to date are

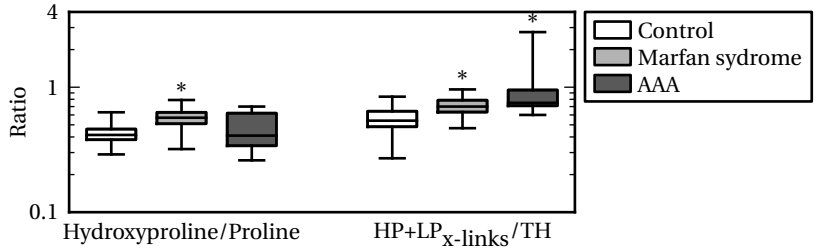

Figure 4.1:
Aortic wall collagen levels were assessed by the hydroxyproline/proline ratio, and the extent of intermolecular collagen cross-links was assessed by the number of hydroxylysyl pyridinoline and lysyl pyridinoline cross-links per triple helix. $*$ $p < 0.00001$.

controversial.[3–5] With the exception of rare mutations in the collagen III gene such as the vascular type of Ehlers-Danlos syndrome, no clear association between impaired collagen homeostasis and aneurysm growth and/or rupture has been identified.

In search of the collagen defect(s) underlying aneurysm formation, we applied an integrated approach of biochemical analyses, multiple imaging modalities, and functional analysis by atomic force microscopy (AFM) to identify the putative collagen defect in aortic abdominal aneurysm (AAA) and in Marfan syndrome, by far the two most common forms of aortic aneurysms. Results of this evaluation show that advanced stages of aneurysmal disease are characterized by distinct defects in the adventitial collagen skeleton armoring the vessel wall rather than by purely biochemical defects.

4.3 Results

Vascular load-bearing collagen is composed of highly stable type I and III fibrillar collagens that are stabilized further by intra-molecular cross-linking.[6] Biochemical as well as morphometric evaluation showed similar collagen concentrations in aneurysm wall from patients with Marfan syndrome and normal, non-aneurysmal control aorta, whereas elevated collagen concentrations were found in AAA (fig. 4.1). The ratio of type I/III collagen MRNA expression was similar in control aorta, Marfan syndrome, and AAA (fig. 4.7). Expression of lysyl oxidase was higher in the aneurysm wall from patients with Marfan syndrome ($p < 0.05$; fig. 4.7). Evaluation of intermolecular collagen cross-linking through quantification of nonreducible lysyl oxidase-initiated collagen cross-links (hydroxylysyl pyridinoline/lysyl pyridinoline cross-links)[7] showed increased intermolecular collagen cross-linking in the aneurysmal wall in both AAA and Marfan tissue (fig. 4.1). These biochemical findings for AAA are in line with reports in the avail-

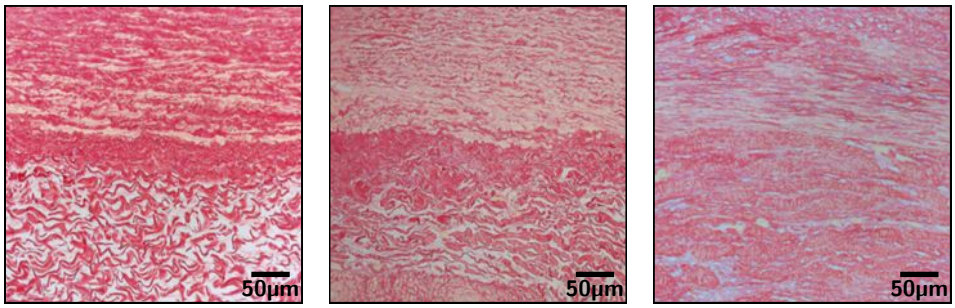

Control Marfan AAA

Figure 4.2:
Collagen deposition (Sirius Red staining) in normal aortic wall and aneurysmal wall in Marfan syndrome and AAA. The images are oriented with the media layer in the upper half and the adventitial layer in the lower half of the image.

able literature, and none of the findings indicates a quantitative or qualitative defect in vascular collagen at the molecular level in AAA or in aneurysms of patients with Marfan syndrome.

In the absence of a clear defect at the biochemical level, we sought for possible structural defects in collagen organization. Histological evaluation (Picro sirius Red collagen staining) (fig. 4.2) and immunohistological staining for collagen type I and III (fig. 4.8) show distinct differences in collagen organization in the medial and adventitial layers of the (grossly) normal aortic wall. A similar pattern but with minor fibrotic changes is seen in the aneurysm wall of patients with Marfan syndrome (fig. 4.2 and fig. 4.8). Collagen deposition in AAA, on the other hand, is hallmarked by complete loss of vessel-wall architecture and deposition of disorganized and condensed collagen (fig. 4.2 and fig. 4.8), a finding that is consistent with fibrosis.

Because the regular 2D images may mask structural defects in the third dimension,[8] we also created 3D reconstructions of the medial and adventitial collagen microarchitecture using the z-stack function on the confocal microscope. These reconstructions show a clearly distinct collagen organization in the medial and adventitial layers of the normal aortic wall (fig. 4.3). Collagen deposition in the medial layer is best characterized by small, interdispersed collagen fibrils that run mainly perpendicular to the circumferential elastic sheets (fig. 4.3A). Adventitial collagen, on the other hand, is arranged in a loose knitting of highly organized ribbon-like collagen bands that brace the medial and intimal layers of the vessel wall (fig. 4.3B). These different architectures appear optimal for achieving the different functionalities for the aortic medial and adventitial layers (elastic recoil and resilience, respectively).[9, 10]

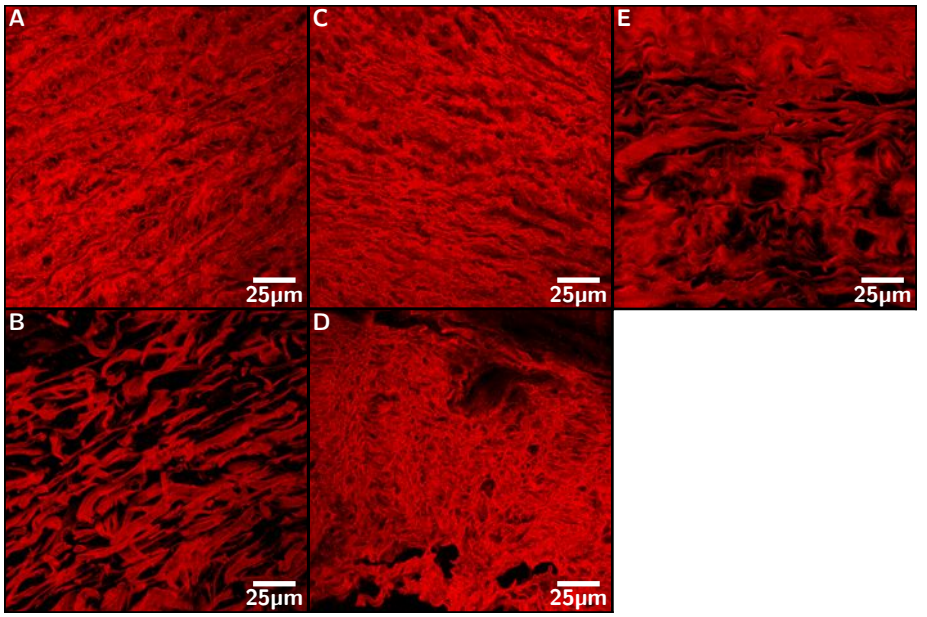

Figure 4.3:
(A,B) Three-dimensional reconstructions (maximum intensity projections of multiple optical sections) of collagen networks in the normal media (A) and adventitial (B) layer.
(C,D) Aneurysms in patients with Marfan syndrome, media (C) and adventitial (D) layer.
(E) Aortic abdominal aneurysm.

Evaluation of collagen architecture in aneurysms of patients with Marfan syndrome showed minor changes in the medial layers of the aortic wall (fig. 4.3C) but a dramatically disturbed collagen architecture in the adventitial layer, with complete absence of the normal collagen fibril organization and deposition of thin parallel collagen fibrils (fig. 4.3D).

Reconstructions for the AAA (fig. 4.3E) show complete loss of the normal architecture, loss of the distinction between medial and adventitial collagen organization, and deposition of aggregated, parallel collagen sheets that appear rigid.

The disordered properties of the collagen microarchitecture in AAA and in the adventitial layer of aneurysms from patients with Marfan syndrome suggest that defects in adventitial collagen organization underlie the weakening of the aortic wall. To test this hypothesis, we performed functional analysis by AFM on normal and aneurysmal adventitial aortic sections. AFM is an established means to test the mechanical properties of individual proteins, cells, and tissue.[11, 12] AFM experiments are performed by indenting the tissue at multiple points with a needle and testing the mechanical response.[13] The tissue response to the

indentation then is used to calculate the elasticity (Young's modulus) for the given point. (The method is described in SI Materials and Methods, section 4.5.) Multiple individual elasticity measurements then are integrated to create a visual representation (stiffness map) of the probed area. The high force resolution of the AFM (in pico-newtons) and its high lateral resolution (i.e., several elasticity measurements per square micrometer) make the AFM ideal for precisely mapping the mechanical properties of tissue at the microscale level, thereby allowing comparison of the elasticity map with the confocal images (fig. 4.3). Moreover, the individual elasticity measurements can be compiled into a histogram that can be used to express the distribution of the elasticity of the arterial wall at a larger scale.

Tissue was probed at two different levels by using different AFM cantilevers: a sharp tip (20 nm end radius) and a blunter ball tip (10 µm radius). These two tips allow a comparison of the different scales in the tissue. The size of the sharp tip is chosen to interact only with individual molecules in the tissue (individual fiber level), whereas the larger ball tip is designed to probe at the tissue level (fibril behavior). The elasticity modulus (Young's modulus) was calculated for each indentation, because then the size and shape of the indenter can be removed, allowing direct comparison of the two measurements. The combined measurements provide a complete picture of the mechanical properties of the tissue and allow the AFM measurements to be compared with previous conventional studies of the mechanical properties of AAA and normal aorta segments.[14, 15] Note, however, that all measurements are performed on a microscale level, not fully loading the fibers.

Stiffness histograms combining the individual data points (fig. 4.4) show that the tissue response of the control adventitia is independent of the size of the tip that is used. This finding indicates that the normal adventitial tissue behaves as a highly coherent network. The stresses encountered by the tissue are dispersed equally over the whole network, and the scale of the challenger does not matter. The fact that the sharp indenter is not able to penetrate the network to a greater extent than the ball tip shows that the individual collagen fibers are densely interconnected, because the fibers do not slide out of the way and are all pulled when a single fiber is moved.

The major difference between the aneurysmal tissues and normal tissue is immediately apparent from the histogram in fig. 4.4 and the AFM force-volume topography (fig. 4.5). Unlike normal tissue, the stiffness of AAA tissue is clearly dependent on the size of the AFM tip: The ball tip, which interacts with the larger structures, senses a very stiff tissue. This observation is in line with our confocal images and conventional biomechanical studies that show that AAA tissue has become stiffer.[16] The sharp tip, on the other hand, meets hardly any resistance,

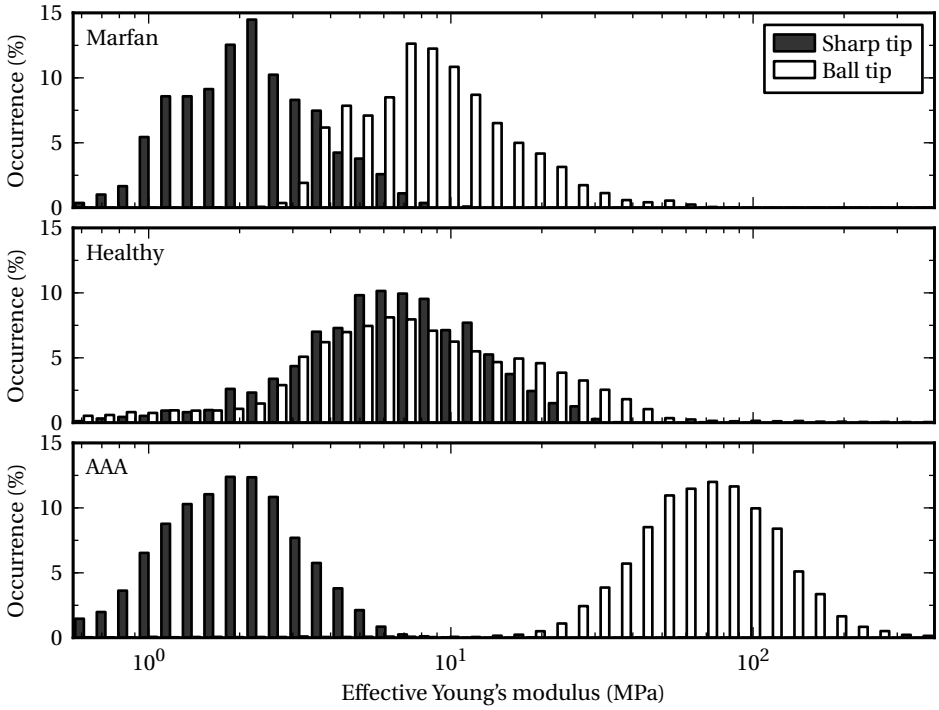

Figure 4.4:
Histograms showing the distribution of the effective Young's modulus for the different conditions. White bars show curves taken with the sharp tip; black bars show curves taken with the ball tip. Values are plotted on a log scale to improve the comparison of the modulus.

suggesting that the sharp tip pushes the fibers of the extracellular matrix aside. This observation indicates that the interconnections that normally allow the tissue to behave as a coherent network are missing in AAA.

Probing of Marfan aneurysmal tissue shows a tissue behavior that is clearly distinct from both control aorta and AAA tissue. The larger ball tip senses stiffness similar to that of normal tissue, suggesting that under the conditions of the AFM experiment (a resting, nonstretched state) the tissue elasticity at a larger scale equals that of normal aortic wall. The sharp tip, on the other hand, finds little resistance and plunges through the tissue just as it did with AAA tissue. This observation indicates that the individual fibers are pushed aside when probed with the 25 nm tip and thus that the loaded fibrils are unable to transfer the stress and strain to the neighboring fibrils (i.e., absence of network behavior).

Another remarkable finding distinct to the Marfan tissue is that sections of the tissue collapse as the force is applied (fig. 4.10). These sections appear to be small voids in the collagen network that also are observed in the confocal images (fig. 4.3D). Such voids could provide sites susceptible to dissection or rupture.[17]

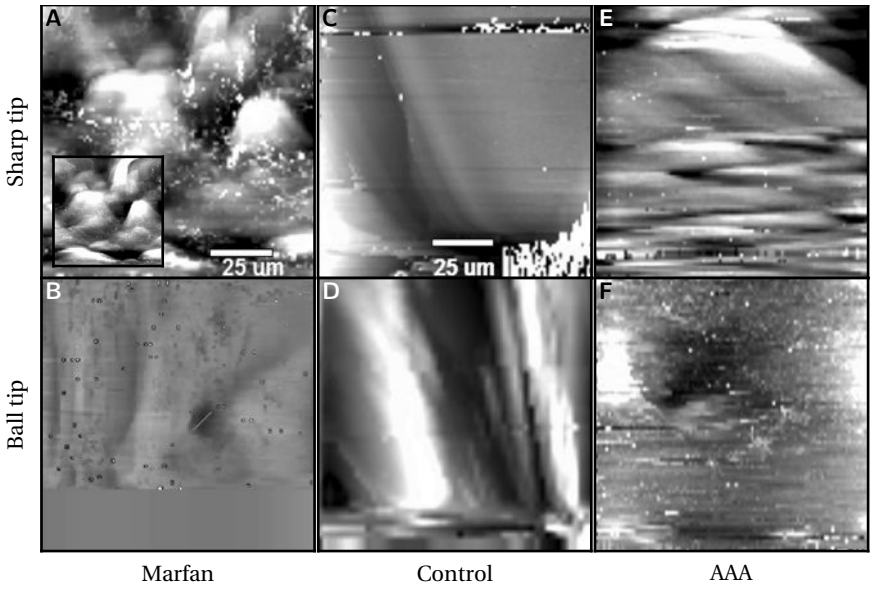

Figure 4.5:
Topography maps for the various tissues as determined from AFM force-volume spectroscopy at 11 nN of constant force. The inset in (A) shows the Marfan tissue at 40 nN; it is apparent that the force collapses something in the tissue at various points resulting in a much smoother-looking surface.

4.4 Discussion

This study shows that advanced aneurysms in AAA and Marfan syndrome are associated more with distinct defects in the collagen microarchitecture than with a collagen defect at the biochemical level. These architectural defects result in loss of the normal stress-strain curve and in impaired collagen network behavior, both of which can contribute to the aortic wall failure.

Visualization of adventitial collagen structures in the control aorta shows a collagen architecture that is best described as a loosely knitted network of interwoven collagen ribbons encasing the medial layer. A similar architecture has been described previously for the adventitial layer of the urine bladder, and it was shown that the collagen ribbons align during bladder filling, thereby allowing the bladder to distend easily but preventing overstretching.[18] The aortic adventitial layer may serve a similar purpose: its flexibility allows the arterial wall to dilate easily but resists overstretching once fully loaded. Such a construction is similar to the textile and metal plies in a steel-belted radial tire that allow flexibility but prevent failure in extreme conditions.

The different architectures of the medial and adventitial layers may well explain

the J-shaped stress-strain curve (i.e., the nonlinearity of the curve) of the normal vessel wall and suggest that the two layers have different functionalities, the elastic medial layer being responsible for the flat, horizontal part of the curve and the adventitial knitting resulting in the steep arm of stress-strain curve.[19]

Visualization of the collagen braiding in Marfan aneurysms and AAA in vessel-wall samples that were obtained at the time of operation (i.e., from advanced stages of the disease) shows that the collagen fibrils run almost in parallel, thereby limiting their ability to stretch, and therefore stiffen the vessel. This observation is well in line with biomechanical studies that show that both AAA and Marfan aneurysms are stiffer than the normal vessel wall.[16, 20]

The increased stiffness of AAA tissue also is immediately apparent from the AFM experiments performed with a ball tip that show a sharp increase in the effective Young's modulus for AAA tissue, indicating that the tissue resisted even the minimal indentations (2–3 µm) by the AFM tip. The similar Young's moduli for ball-tip experiments in normal aorta and aortas from patients with Marfan syndrome seemingly conflict with biomechanical studies that indicate that Marfan tissue is stiffer than normal tissue.[20] This apparent contradiction presumably reflects a limitation when AFM measurements are performed under resting, nonstretched conditions. The confocal images clearly show that under such conditions collagen fibrils in Marfan tissue adopt a wave-like pattern that allows them to stretch when probed with the AFM tip.

Findings from this study also point to defects in collagen network behavior in the aneurysmal tissues studied. Network behavior has long been recognized as a key to mechanical stability in the field of structural design, but, remarkably, in the biomedical context network behavior has only been reported for bone tissue.[12] Our results indicate that aneurysms in both AAA and Marfan tissue are associated with defects at all three scale lengths (i.e., at the intrafibril, intrafiber, and suprafiber levels). Impaired network behavior may interfere with the dissipation of the mechanical forces over the arterial wall, thereby contributing further to the mechanical failure of the aortic wall.

In conclusion, the findings in this study provide a structural explanation of how biological tissue (i.e., normal arterial wall) can acquire its typical nonlinear stress-strain curve and also can settle the longstanding controversy regarding the existence of a collagen deficiency in AAA. We show that defects in collagen architecture and network behavior, rather than a defect at the molecular level, explain the debilitation of the aortic wall in AAA and aneurysms in Marfan syndrome. The observed changes in AAA do not necessarily reflect the primary cause of AAA formation. More likely, the changes in AAA reflect inappropriate collagen deposition (fibrosis) in an environment that is characterized by sustained inflammation and activation of multiple proteolytic pathways. The findings in Marfan syndrome, on

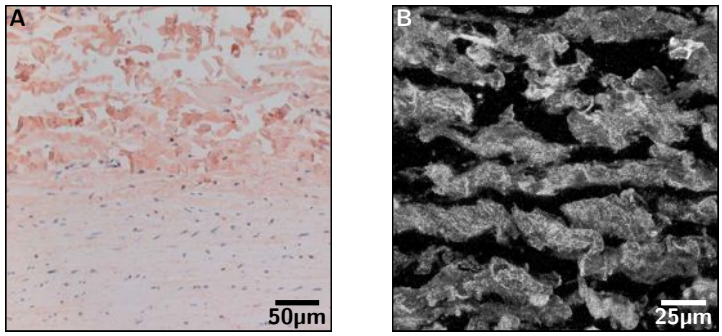

Figure 4.6:
Fibrillin localization in the normal aortic wall (immunohistochemistry).
(A) Fibrillin (reddish-brown) is present primarily in the adventitial layer of the aortic wall.
(B) Three-dimensional reconstruction by confocal microscopy showing that fibrillin colocalizes with adventitial collagen.

the other hand, may reflect a primary defect: Unlike AAA, aneurysms in patients with Marfan syndrome do show signs of increased inflammation and proteolytic activities.[21] As such, the observed defects in the collagen microarchitecture may reflect a primary defect that could relate to impaired TGF-β signaling. However, the strong link between a defect in the fibrillin gene and development of Marfan syndrome also may reflect a role of fibrillin in the organization of the collagen bands in the adventitial layer. This notion is supported by the fact that fibrillin is localized predominantly in the adventitia of the normal aortic wall (fig. 4.6A) and by the pattern of fibrillin deposition that is similar to that of the adventitial collagen network (fig. 4.6B). Our findings confirm the longstanding assumption that Marfan syndrome is a collagen disorder[22] and show that Marfan syndrome is associated with a defect in collagen network organization. Such a defect may well explain most of the other phenotypical features of Marfan syndrome which appear related to collagen dysfunction (e.g., skeletal deformities, hernias, dural ectasia, and ectopia lentis).

We speculate that defects similar to those in AAA explain the longstanding apparent contradiction between increased collagen content but reduced mechanical strength during wound healing and scar formation.[23] Microarchitectural defects in collagen network formation may well contribute to scar formation in postfetal wound healing that currently is attributed to a reduced elastin transcription after birth.[24]

4.5 Materials and Methods

All human arterial wall samples were provided by the Vascular Tissue Bank, Department of Vascular Surgery, Leiden, The Netherlands. Sample collection and handling was performed in accordance with the guidelines of Medical Ethical Committee of the Leiden University Medical Center, Leiden, The Netherlands, and the code of conduct of the Dutch federation of Biomedical Scientific Societies.[25]

Anterior lateral aneurysm wall samples were obtained from patients with an AAA > 55 mm undergoing elective open repair (AAA group: $n = 17$, mean age 72.4 ± 6.2 years). Thoracic aortic aneurysms (ascending aorta, diameter > 50 mm) of Marfan patients were obtained during elective repair (Bentall procedures) (Marfan group: $n = 11$, age 26.9 ± 8.2 years). All Marfan patients met the international criteria for Marfan syndrome.[26]

Control (normal) abdominal aortic wall was obtained during kidney explantation for organ donation. All these control samples were obtained from the level of the renal artery, i.e., from a location comparable to that of the samples from AAA patients ($n = 11$, age 55.6 ± 10.2 years). The primary cause of the fatal brain injury in this control group was a major head trauma or subarachnoidal bleeding.

Control thoracic aorta (post mortems) from patients dying from noncardiac causes was used as a histological reference for the Marfan tissue.

Following excision, half of the sample was fixed in formalin for 24 h, decalcified in Kristensen's solution, and subsequently embedded in paraffin for immunohistochemical analysis. The remaining half was immediately flash-frozen in liquid nitrogen for mRNA analysis and for the preparation of cryosections.

Details on the biochemical, histological, and AFM methodology and reproducibility (fig. 4.9), and statistical analysis are provided in SI Materials and Methods.

4.6 Supporting Information

SI Materials and Methods

Collagen and Cross-Link Analysis. Ten 10 μm slices of paraffin-embedded tissue were deparafinized in xylene, and the samples were hydrolyzed (110 °C, 20–24 h) in 1 mL 6 M HCl in 5 mL Teflon-sealed glass tubes. The samples were dried and redissolved in 1 mL of water containing 10 μM of pyridoxine [internal standard for the cross-links hydroxylysylpyridinoline (HP) and lysyl-pyridinoline] and 2.4 mmol/L of homoarginine (internal standard for amino acids) (Sigma). Samples were diluted 5-fold with 0.5% (vol/vol) heptafluorobutyric acid (Fluka) in

10% (vol/vol) acetonitrile for cross-link analysis; aliquots of the 5-fold diluted sample were diluted 50-fold with 0.1 M sodium borate buffer (pH 8.0) for amino acid analysis. Derivatization of the amino acids with 9-fluorenylmethyl chloroformate and reversed-phase HPLC of amino acids and cross-links was performed on a Micropak ODS-80TM column (150 mm × 4.6 mm) (Varian) as described previously.[27, 28] The quantities of the cross-link HP were expressed as the number of residues per collagen molecule, assuming 300 hydroxyproline (Hyp) residues per triple helix. This procedure is well established, because Hyp is a collagen-specific amino acid and because the prolyl hydroxylation level in collagen is stable.

RNA Extraction and mRNA Analysis. Total RNA extraction was performed using RNAzol (Campro Scientifics) and glass beads according to the manufacturer's instructions. Copy-DNA was prepared using kit #A3500 (Promega), and quantitative realtime PCR analysis was performed for collagen type I and III and lysyl oxidase on the ABI-7700 system (Applied Biosystems) using established primer/probe sets (Assays on Demand; Applied Biosystems) and MasterMix (Eurogentec). Analyses were performed according to the manufacturers' instructions and as previously reported.[29] GAPDH expression was used as a reference and for normalization.

Histology. Histochemistry and immunohistochemistry was performed on 4 µm deparaffinized, ethanol-dehydrated tissue sections. Collagen staining was performed by the Sirius Red-picrine method.[30] Immunohistochemical staining for collagen type I and III and fibrillin was performed using specific antibodies for collagen type I (C7510-17K; US Biological), collagen type III (C7510-39G; US Biological), or fibrillin (MAB1919, Chemicon). Pepsin-trypsin retrieval was required for optimal collagen I and III staining, and a 10 mM (pH 6.0) citrate retrieval was required for the fibrillin staining.

AB-conjugated biotinylated anti-goat or rabbit anti-IgG was used as secondary antibody. Sections were stained with Nova Red (Vector Laboratories) and counterstained with Mayer's hematoxylin. Controls were performed by omitting the primary antibody.

We used confocal microscopy (LSM615; Zeiss) for the visualization of the collagen network structures. Tissue slices (20 µm) were stained with Sirius Red, and Sirius Red fluorescence was used for the reconstruction. Fibrillin deposition was evaluated by immunohistochemical staining (see above) using the Alexa 647 mouse anti-goat antibody for visualization. Serial confocal sections of x-y images (stack size 206 µm × 206 µm) of representative sections of the medial and adventitial layer were made along the z axis with a distance of 0.5 µm. The excitation

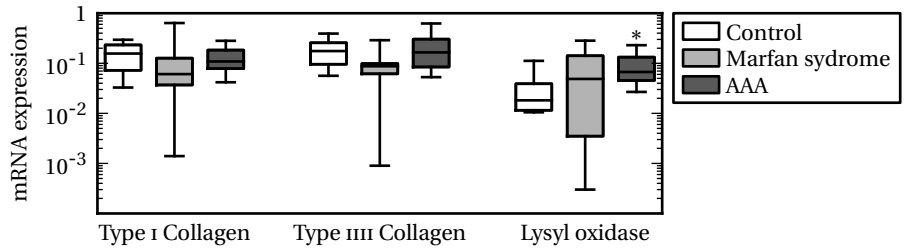

Figure 4.7:
mRNA expression relative to GAPDH (GAPDH = 1) of type I and III collagen, and lysyl oxidase (a key enzyme required for collagen cross-linking). $*$ $p < 0.00001$.

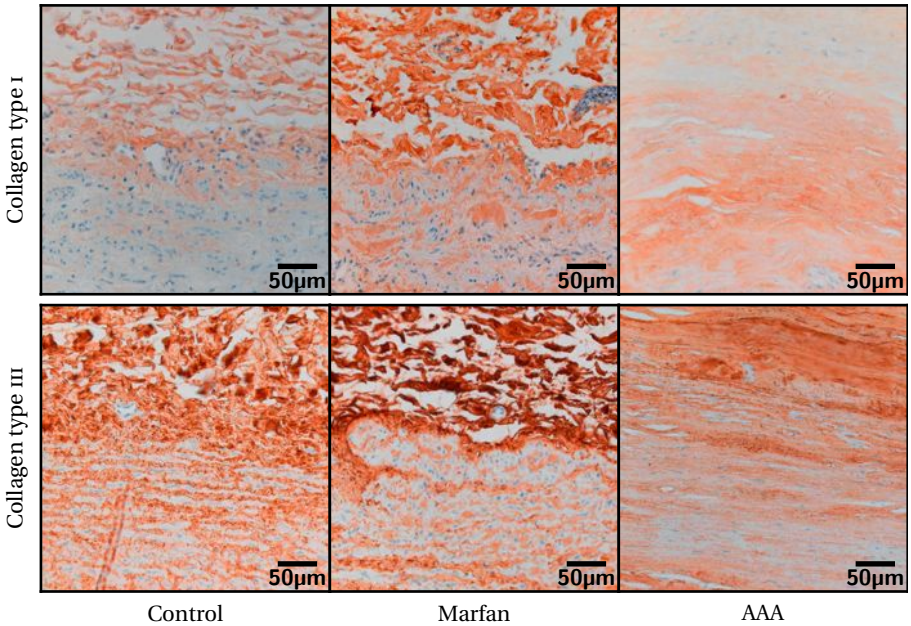

Figure 4.8:
Collagen type I and III distribution in medial-adventitial border zone of control (abdominal) aorta, ascending aortic aneurysm in Marfan syndrome, and AAA.

and emission wavelengths were 543 and 633 nm, respectively, for the Sirius Red staining and were 633 and 647 nm, respectively, for immunohistochemical (Alexa 647) staining. The pinhole was set at 108 µm. Three-dimensional reconstructions of confocal stacks (20 serial images at 0.5 µm intervals) were performed using the stacks-z-function on the Zeiss LSM Image Examiner version 3.2.0.115.

Atomic Force Microscopy. Atomic force microscopy (AFM) measurements were performed on 8 µm-thick tissue slices. To that end, tissue was cryosliced to 8 µm thickness, perpendicular to the flow of the blood, and stored at −80 °C. Measurements were done using a Molecular Imaging PicoScan atomic force microscope controlled with a custom scripting program written in LabVIEW (National Instruments) and Visual Basic 6 (Microsoft). Data were recorded with a National Instruments card at 100 kS/s and then processed into higher-resolution force-volume images than can be taken with the control software of the AFM. All force-distance curves were performed at a rate of 1 Hz.

Tissue was probed at two different resolutions: A sharp tip (20 nm tip radius) was used to probe the tissue on the fibril level, and a 10 µm ball tip was used to probe at the tissue level.[31, 32] The sharp tips were Nanoprobe tips model NP (Veeco). Cantilevers were calibrated using the thermal method.[33]

Balls tips were specially modified tips from Novascan. These tips are Park cantilevers (Veeco) to which a 10 µm glass ball is attached. Because the effective stiffness of the tissue is greater when probed at a larger scale, we choose cantilevers with a force constant of 0.32 N/m. Tips were coated by a layer of polyethylene glycol (molecular weight 3,400 kDa) to prevent fouling.

All AFM measurements were performed in a liquid cell (Molecular Imaging) in PBS. Preliminary evaluation showed that the AFM measurements on the aorta sections were independent of the spring constant of the cantilevers. Consistency of the data was checked by measuring the variations in stiffness in a number of healthy individuals. As shown in fig. 4.9, the variation among the individuals tested is consistent with the conclusion that the differences found among different tissues are disease specific rather than representing variation among individuals.

AFM Function and Nanoindentation. Force-extension curves were performed by laying a section of tissue on a glass slide and immersing it in the PBS buffer in the liquid cell. Tissue then was loaded in the AFM microscope, and a force-volume dataset was produced by pushing the cantilever into the tissue at each point on a grid. This technique allowed the collection of a 2D grid of indentation data that then was transformed as explained below into effective Young's modulus as well

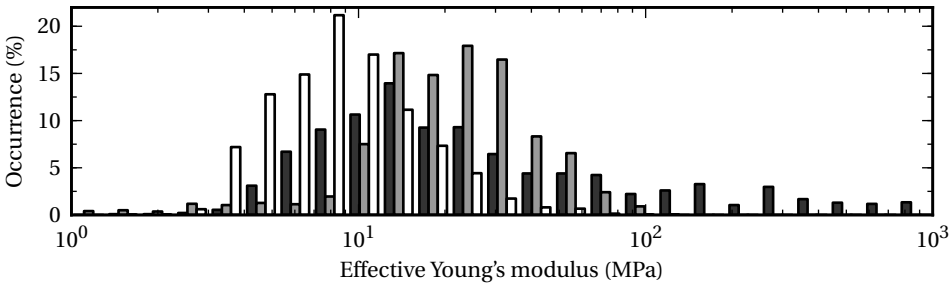

Figure 4.9:
Force distribution of three distinct healthy aortas (black, gray and white bars) measured by the sharp tip.

as a constant-force topograph.

The Young's modulus was determined using the methods of A-Hassan et al.[34] This technique is more robust to the errors that are inherently present in fitting the Hertz model[35] of an indenter to data collected from AFM force-distance curves. A detailed discussion of the methods that can be used to find the Young's modulus from AFM force-extension curves can be found in Stolz et al.[36] or in A-Hassan et al.[34] This technique involves determining the work performed by the cantilever on the tissue sample and then comparing this work with a known standard. By integrating the total area under the force-distance curve, local variations are minimized, and the curve fitting becomes less difficult. Most importantly, the exact point of contact between surface and AFM cantilever is no longer needed, because the area under the curve at the estimated contact point is small compared with the total area under the curve. Its ease of application and, more importantly, its reproducibility, make this technique the more desirable method of determining the effective Young's modulus of the tissue.

In this case, Sneddon's equations[37] were used to estimate the curve that would be expected with a conical (sharp tip) or spherical (ball tip) Hertz model indenter. Although this estimation negates some of the advantages of this method, namely the ability to divide the shape, force constant, and sensitivity of the tip from the equation, it still produces a standard curve to which all of the curves analyzed by this method have been compared. Thus, although the absolute value for the Young's modulus has a large error, the error is systematic, and comparisons between the various datasets are still completely valid.

Validity and Reproducibility of the AFM Measurements. Two different force constants were used between the ball tips and the sharp tips. To determine what effects the differing force constants would have, we performed an experiment

with the sharp tip on aortic abdominal aneurysm (AAA) tissue. Various cantilevers were available on the nanoprobe chip; we used cantilevers with the 0.06 N/m and the 0.32 N/m tips, force constants that were chosen specifically to match the stiffness of the tissue and therefore to maximize the force resolution.

The effect from the force constant of the cantilever over this range is negligible. The observed differences pale in comparison with the differences between the Marfan and AAA tissue. Therefore we can safely assume that the differences seen in the aneurysmal tissue between the ball tip and the sharp tip result solely from the differences in tip shape.

Action of Ball Tip vs. Sharp Tip. The different-sized tips allow very different information about the collagen networks to be collected, and the data provide a sense of the coherence of the matrix network. The two tips allow an understanding of the collagen networks as well as interacting directly with individual proteins. The sharper tip is smaller than the radius of a collagen fibril. It is able to interact directly with these structures in the extracellular matrix as well as slip between the fibers. The ball tip was chosen to interact with the tissue on a micrometer scale. This tip is able to push tens of fibers and directly measures the network indentation properties of the tissue. The size is a compromise between seeing the large network behavior and yet remaining small enough to handle with an AFM tip.

Nanoindentation Stiffness Maps. The force-vs.-distance curves were processed into a combination topography and stiffness image by combining all the force-extension curves from the AFM measurements into a grid and then taking the extension at which the force reached a certain level as the intensity at that point. This method is sensitive to both the initial height of the tissue and to the stiffness of the tissue under the cantilever. Regions where the tissue is stiffer will indent less before the required force is reached and will therefore appear higher than regions that were equally high before indentation but that are softer. We find that these images provide information complementary to the collagen confocal images.

Statistics. Differences between the groups were evaluated by an unpaired t test (for the normally distributed data) or by the Wilcoxon-Mann-Whitney test (for non-normally distributed continuous data). The level of significance was set at $p < 0.05$. All analyses were performed using SPSS16.0 (SPSS Inc.)

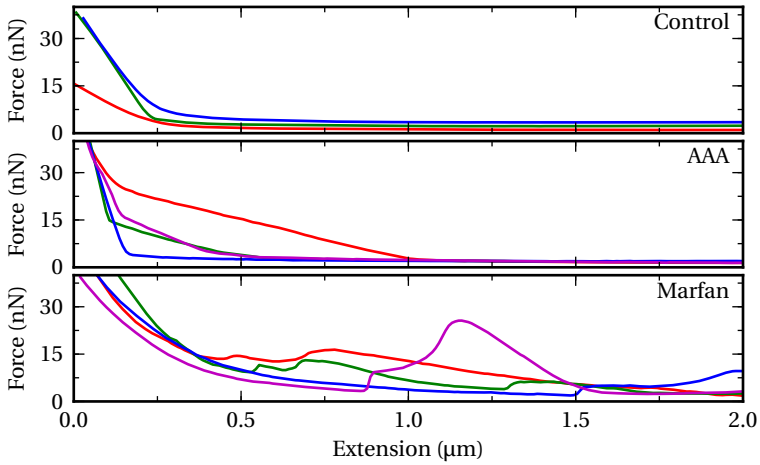

Figure 4.10:
Individual force extension curves. "Extension" refers to the length of the piezoelectric tube. Motion toward zero results in indentation of the tissue by the cantilever tip. (Top) Curves sampled from control tissue. (Middle) Curves sampled from AAA tissue showing the nonlinear interactions common on the AAA tissue with the ball tip. It is proposed that the nonlinearity is a result of one collagen fiber being pushed into a second fiber, resulting in markedly stronger forces with nonlinear transitions at the connection. This behavior is consistent with the notion that there are fewer interconnections between the various collagen fibers resulting in no warning for the second fiber and its sudden recruitment. (Bottom) Curves sampled from Marfan tissue showing the collapses that are common with the Marfan tissue. These collapses could be the result of the weakened collagen fibers slipping to the side of the tip or could indicate structural weaknesses in the tissue. The confocal images in fig. 4.3A and B show the presence of small voids.

4.7 References

[1] N. Sakalihasan, R. Limet, and O. Defawe. Abdominal aortic aneurysm. *Lancet*, 365:1577, 2005.

[2] R. W. Thompson, P. J. Geraghty, and J. Lee. Abdominal aortic aneurysms: Basic mechanisms and clinical implications. *Curr. Prob. Surg.*, 39:98, 2002.

[3] G. McGee, et al. Aneurysm or occlusive disease - factors determining the clinical course of atherosclerosis of the infrarenal aorta. *Surgery*, 110:370, 1991.

[4] R. J. Rizzo, et al. Collagen types and matrix protein content in human abdominal aortic aneurysms. *J. Vasc. Surg.*, 10:365, 1989.

[5] S. Menashi, J. S. Campa, R. M. Greenhalgh, and J. T. Powell. Collagen in abdominal aortic aneurysm: typing, content, and degradation. *J. Vasc. Surg.*, 6:578, 1987.

[6] S. M. Sweeney, et al. Candidate cell and matrix interaction domains on the collagen fibril, the predominant protein of vertebrates. *J. Biol. Chem.*, 283:21187, 2008.

[7] H. M. Kagan and W. Li. Lysyl oxidase: properties, specificity, and biological roles inside and outside of the cell. *J. Cell. Biochem.*, 88:660, 2003.

[8] J. Alkemper and P. W. Voorhees. Quantitative serial sectioning analysis. *J. Microsc*, 201:388, 2001.

[9] P. B. Dobrin, W. H. Baker, and W. C. Gley. Elastolytic and collagenolytic studies of arteries. Implications for the mechanical properties of aneurysms. *Arch. surg.*, 119:405, 1984.

[10] T. Inahara. Eversion endarterectomy for aortoiliofemoral occlusive disease. A 16 year experience. *Am. J. Surg.*, 138:196, 1979.

[11] T. Ludwig, R. Kirmse, K. Poole, and U. S. Schwarz. Probing cellular microenvironments and tissue remodeling by atomic force microscopy. *Pflugers Arch.*, 456:29, 2008.

[12] G. E. Fantner, et al. Sacrificial bonds and hidden length dissipate energy as mineralized fibrils separate during bone fracture. *Nat. Mater.*, 4:612, 2005.

[13] N. Gadegaard. Atomic force microscopy in biology: technology and techniques. *Biotech. Histochem.*, 81:87, 2006.

[14] J. F. Rodríguez, C. Ruiz, M. Doblaré, and G. A. Holzapfel. Mechanical stresses in abdominal aortic aneurysms: influence of diameter, asymmetry, and material anisotropy. *J. Biomech. Eng.*, 130:021023, 2008.

[15] D. A. Vorp and J. P. Vande Geest. Biomechanical determinants of abdominal aortic aneurysm rupture. *Arterioscler. Thromb. Vasc. Biol.*, 25:1558, 2005.

[16] C. M. He and M. R. Roach. The composition and mechanical properties of abdominal aortic aneurysms. *J. Vasc. Surg.*, 20:6, 1994.

[17] N. M. Ammash, T. M. Sundt, and H. M. Connolly. Marfan syndrome-diagnosis and management. *Curr. Probl. Cardiol.*, 33:7, 2008.

[18] S. L. Chang, P. S. Howard, H. P. Koo, and E. J. Macarak. Role of type III collagen in bladder filling. *Neurourol. Urodyn.*, 17:135, 1998.

[19] R. E. Shadwick. Mechanical design in arteries. *J. Exp. Biol.*, 202:3305, 1999.

[20] B. Sonesson, F. Hansen, and T. Länne. Abnormal mechanical properties of the aorta in Marfan's syndrome. *Eur. J. Vasc. Surg.*, 8:595, 1994.

[21] M. J. Collins, et al. Variation in the histopathological features of patients with ascending aortic aneurysms: a study of 111 surgically excised cases. *J. Clin. Pathol.*, 61:519, 2008.

[22] M. Macek, J. Hurych, M. Chvapil, and V. Kadlecová. Study of fibroblasts in Marfan's syndrome. *Humangenetik*, 3:87, 1966.

[23] J. Madden. *Textbook Of Surgery; The Biological Basis Of Modern Surgical Practice.* Wound healing (W. B. Saunders, Philadelphia, 1986).

[24] M. T. Longaker and N. S. Adzick. The biology of fetal wound healing: a review. *Plast. Reconstr. Surg.*, 87:788, 1991.

[25] Code of conduct of the Dutch federation of Biomedical Scientific Societies, http://www.federa.org/?s=1&m=78&p=&v=4.

[26] A. De Paepe, et al. Revised diagnostic criteria for the Marfan syndrome. *Am. J. Med. Genet.*, 62:417, 1996.

[27] R. A. Bank, E. J. Jansen, B. Beekman, and J. M. te Koppele. Amino acid analysis by reverse-phase high-performance liquid chromatography: improved derivatization and detection conditions with 9-fluorenylmethyl chloroformate. *Anal. Biochem.*, 240:167, 1996.

[28] R. A. Bank, et al. Sensitive fluorimetric quantitation of pyridinium and pentosidine crosslinks in biological samples in a single high-performance liquid chromatographic run. *J. Chromatogr. B Biomed. Sci. Appl.*, 703:37, 1997.

[29] H. Abdul-Hussien, et al. Collagen degradation in the abdominal aneurysm: a conspiracy of matrix metalloproteinase and cysteine collagenases. *Am. J. Pathol.*, 170:809, 2007.

[30] L. C. Junqueira, G. Bignolas, and R. R. Brentani. Picrosirius staining plus polarization microscopy, a specific method for collagen detection in tissue sections. *Histochem. J.*, 11:447, 1979.

[31] P. D. Kemp and J. E. Scott. Ehrlich chromogens, probable cross-links in elastin and collagen. *Biochem. J.*, 252:387, 1988.

[32] S. R. Pinnell and G. R. Martin. The cross-linking of collagen and elastin: enzymatic conversion of lysine in peptide linkage to alpha-aminoadipic-delta-semialdehyde (allysine) by an extract from bone. *PNAS*, 61:708, 1968.

[33] J. L. Hutter and J. Bechhoefer. Calibration of atomic-force microscope tips. *Rev. Sci. Instrum.*, 64:1868, 1993.

[34] E. A-Hassan, et al. Relative microelastic mapping of living cells by atomic force microscopy. *Biophys. J.*, 74:1564, 1998.

[35] H. Hertz. Ueber die Berührung fester elastischer Körper. *Journal für die reine und angewandte Mathematik (Crelles Journal)*, 1882:156, 1882.

[36] M. Stolz, et al. Dynamic elastic modulus of porcine articular cartilage determined at two different levels of tissue organization by indentation-type atomic force microscopy. *Biophys. J.*, 86:3269, 2004.

[37] I. N. Sneddon. The relation between load and penetration in the axisymmetric Boussinesq problem for a punch of arbitrary profile. *Int. J. Eng. Sci.*, 1965.